research articles Journal of proteome research

The Proteomic Response of *Mycobacterium smegmatis* to Anti-Tuberculosis Drugs Suggests Targeted Pathways

Rong Wang[†] and Edward M. Marcotte*

Center for Systems and Synthetic Biology, Institute of Cellular and Molecular Biology, and Department of Chemistry and Biochemistry, University of Texas at Austin, 2500 Speedway, MBB 3.210 Austin, Texas 78712

Received May 22, 2007

Mycobacterium smegmatis is a fast-growing model mycobacterial system that shares many features with the pathogenic *Mycobacterium tuberculosis* while allowing practical proteomics analysis. With the use of shotgun-style mass spectrometry, we provide a large-scale analysis of the *M. smegmatis* proteomic response to the anti-tuberculosis (TB) drugs isoniazid, ethambutol, and 5-chloropyrazinamide and elucidate the drugs' systematic effects on mycobacterial proteins. A total of 2550 proteins were identified with ~5% false-positive identification rate across 60 experiments, representing ~40% of the *M. smegmatis* proteome (~6500 proteins). Protein differential expression levels were estimated from the shotgun proteomics data, and 485 proteins showing altered expression levels in response to drugs were identified at a 99% confidence level. Proteomic comparison of anti-TB drug responses shows that translation, cell cycle control, and energy production are down-regulated in all three drug treatments. In contrast, systems related to the drugs' targets, such as lipid, amino acid, and nucleotide metabolism, show specific protein expression changes associated with a particular drug treatment. We identify proteins involved in target pathways for the three drugs and infer putative targets for 5-chloropyrazinamide.

Keywords: Mycobacterium • mass spectrometry • tuberculosis • drug targets

Introduction

Tuberculosis (TB) is one of the most prevalent infectious diseases in the world, claiming 2 million lives every year.[1] Lengthy chemotherapy and emergence of drug-resistant strains pose significant problems for effective control. To shorten the duration of TB therapy, novel drugs are needed against the causative agent of TB, *Mycobacterium tuberculosis*. Understanding the biological action of the current drugs should help in the development of new drugs. Isoniazid (INH), ethambutol (EMB), and pyrazinamide (PZA) (Figure 1) are the front-line drugs currently used to treat TB.[2] INH selectively inhibits the synthesis of mycolic acids, the main component of the waxy cell wall in mycobacteria.[3] Both enoyl-acyl carrier protein reductase (InhA) and 3-oxoacyl-acyl carrier protein synthase 2 (KasB) have been proposed as the primary targets of INH, which are involved in the type II fatty acid synthase (FAS II) system of mycobacteria for full-length extension of the meromycolate chain.[4] The primary target of EMB is arabinosyl transferase (EmbABC), which is responsible for the synthesis of the arabinan portion of arabinogalactan (AG)[5] and lipoarabinomannan (LAM)[6,7] in mycobacterial cell walls. PZA disrupts cell membrane function and depletes energy transport.[2,8] Relatively little is known about the specific targets of PZA, although fatty acid synthase (Fas) has been proposed as a potential target.[9]

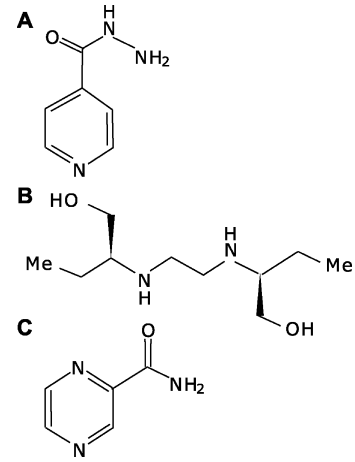

Figure 1. Structures of the anti-TB drugs isoniazid (A), ethambutol (B), and pyrazinamide (C).[2]

Proteomics is capable of investigating the systematic response of cells in a reasonably comprehensive manner[10] and is readily applied to mycobacteria. With the use of two-dimensional gel electrophoresis coupled with mass spectrometry (2DE-MS), a total of 263 proteins were identified in *M. tuberculosis* and *Mycobacterium bovis* BCG strains.[11] In *M. tuberculosis*, Schmidt et al. identified 108 proteins[12] and Sinha

* To whom correspondence should be addressed. E-mail: marcotte@icmb.utexas.edu.

† Current address : Pathogen Functional Genomics Resource Center, J. Craig Venter Institute, 9712 Medical Center Drive, Rockville, MD 20850.

10.1021/pr0703066 CCC: $37.00
Published on Web 02/15/2008

et al. identified 105 membrane proteins.[13] With the use of multidimensional chromatographic separation and mass spectrometric detection (LC/LC/MS/MS or MUDPIT (Multidimensional Protein Identification Technology)),[14] 1044 proteins were identified from three subcellular compartments in *M. tuberculosis*[15] and 901 proteins were identified from *Mycobacterium smegmatis*.[16]

Protein profiles after exposure to drugs make it possible to classify compounds of unknown mechanism of action into similar groups, thereby elucidating the site of drug action.[5] We employed quantitative mass spectrometry to compare proteomic fingerprints of anti-TB drugs and to identify markers of drug action. Specifically, we examined the fast-growing *M. smegmatis*, a nonpathogenic model system for studying the cellular processes of mycobacteria, such as the related pathogenic species *M. tuberculosis*. *M. smegmatis* has previously been used to study alterations in protein expression in anti-TB drug treatments and is sensitive to INH,[17] EMB,[18] and PZA's analogue 5-Cl-PZA,[9] but resistant to PZA. With LC/LC/MS/MS, we measured the global response of the *M. smegmatis* proteome to INH, EMB, and 5-Cl-PZA, which enabled us to identify proteins that show altered expression levels and elucidate the drugs' systematic effects on mycobacterial cells.

Experimental Procedures

Growth and Drug Treatment of *M. smegmatis* Cells. *M. smegmatis* mc^{2}155 bacteria were grown with agitation at 37 °C in Middlebrook 7H9 broth (Difco, supplemented with 10% Middlebrook ADC enrichment, 0.2% glycerol, and 0.05% Tween-80) to midexponential phase.[19] Cultures for experimental treatment were initiated by diluting 1:200 into fresh 7H9 media and grown to early log phase ($OD_{600} \approx 0.3$) with shaking in 5% CO_2 atmosphere at 37 °C. Drug treatments were begun by adding filtered stock solutions of INH (10 mg/mL, Sigma) or EMB (10 mg/mL, Sigma) to achieve the following final concentrations of 4, 8, 12, 16, and 30 μg/mL for INH and 0.5, 1, 2, 4, and 8 μg/mL for EMB.[20] Minimum inhibitory concentrations (MICs) were verified using the microbroth dilution technique,[21] by testing 7 drug concentrations (bracketing the published MIC values), each tested by 12 replicates. 5-Cl-PZA treatment was performed in Middlebrook 7H9 media adjusted to pH 5.6 with HCl when cultures were grown from OD_{600} of 0.2,[22,23] with final 5-Cl-PZA concentrations of 25 and 50 μg/mL. Measured MICs are in agreement with the literature values: 4 μg/mL for INH, 1 μg/mL for EMB, and 25 μg/mL for 5-Cl-PZA.[8,24,25] Samples were collected at selected intervals as in ref 20. In addition to 25 samples from ref 16, 2 more untreated control samples were collected at OD_{600} of 1.9 from Middlebrook 7H9 media. Samples were centrifuged at 12 000*g* for 30 min, suspended in ice-cold lysis buffer (25 mM Tris HCl, pH 7.5, 2.5 mM DTT, 1.0 mM EDTA, and 1× Calbiochem Protease Inhibitor Cocktail Set I (CPICSI)) (1 mL/g cell pellet), and disrupted by bead-beating with 0.1 mm glass beads.[26,27] Cell lysates were clarified by centrifugation at 20 000*g* for 30 min, with typical protein concentrations of 10 mg/mL.

Preparation and LC/LC/MS/MS Analysis of *M. smegmatis* Peptides. *M. smegmatis* soluble protein extracts were diluted in digestion buffer (50 mM Tris HCl, pH 8.0, 1.0 M urea, and 2.0 mM $CaCl_2$), denatured at 95 °C for 15 min, and digested with sequencing grade trypsin (Sigma) at 37 °C for 20 h. Untreated control samples were analyzed as in ref 16. Tryptic peptide mixtures were separated by automated two-dimensional high performance liquid chromatography. Chromatography was performed at 2 μL/min with all buffers acidified with 0.1% formic acid. A BioBasic-SCX 100 × 0.32 (mm) column was used for first-dimensional peptide separation. Chromatographic salt step fractions were eluted from the strong-cation exchange column with a continuous 5% acetonitrile (ACN) background and 10 min salt bumps of 5, 20, 60, and 900 mM ammonium chloride. Each salt bump was eluted directly onto a C18 reverse-phase column and washed free of salt. Reverse-phase chromatography was run in a 125 min gradient from 5% to 50% ACN, then purged at 95% ACN. Peptides were analyzed online with electrospray ionization ion trap mass spectrometry[1,14,28] using a ThermoFinnigan Surveyor/DecaXP+ instrument. For drug-treated samples, gas phase fractionation was used to achieve maximum proteome coverage and increase coverage of low-abundance proteins.[29] Three sequential LC/LC/MS/MS analyses were performed, with spectra collected from different mass/charge (m/z) ranges (300–650, 650–1000, and 1000–1500 m/z) during data-dependent precursor ion selection. For each MS spectra, the 5 tallest individual peaks, corresponding to peptides, were fragmented by collision-induced dissociation with helium gas to produce MS/MS spectra, using a normalized collision energy setting of 34%. Fragmentation data from each set of three runs were combined for peptide analysis. ESI voltage was set at 3.2 kV and capillary heated to 160 °C.

Protein Identification. For peptide and protein identification purposes, we used a database of 8968 potential *M. smegmatis* coding sequences described in ref 16. Mass spectrometry data were analyzed using the data processing program BioWorks Turbosequest 3.1. Proteins were identified from the resulting peptide MS/MS fragmentation spectra by searching against the custom *M. smegmatis* predicted protein database using BioWorks Turbosequest 3.1, considering up to 2 missed tryptic cleavages. The unique and total number of peptides for each identified protein in a given proteomics experiment were obtained using PeptideProphet[30] and ProteinProphet,[31] implemented in the Transproteomic Pipeline v.1.2.3. Proteins were identified with a 5% false-positive identification rate using the ProteinProphet error model. The mass spectrometry raw data from this study, along with all database search parameters, have been deposited in the Open Proteomics Database,[32] under accession nos. opd00007_MYCSM-opd00031_MYCSM and opd00052_MYCSM-opd00086_MYCSM.

Protein Quantification. To estimate the relative abundance of each protein *i*, we employed the differential Absolute Protein Expression measurement (APEX) technique:[33,34] we counted the number (n_i) of observed MS/MS spectra associated with each identified protein and calculated relative protein abundance f_i for that experiment as $f_i = n_i/N$, where N is the total number of observed MS/MS spectra in the experiment. On the basis of these measures of f_i, the significance of differential protein expression was calculated using a Z-score as

$$Z = \frac{f_{i,1} - f_{i,2}}{\sqrt{f_{i,0}(1 - f_{i,0})/N_1 + f_{i,0}(1 - f_{i,0})/N_2}}$$

where the numerator represents the difference in sampled proportions of protein *i* in two shotgun proteomics experiments $f_{i,1} = n_{i,1}/N_1$, $f_{i,2} = n_{i,2}/N_2$; and the denominator represents the standard error of the difference under the null hypothesis in which the two sampled proportions are drawn from the same underlying distribution with the overall proportion, $f_{i,0} = [(n_{i,1} + n_{i,2})/(N_1 + N_2)]$. In this analysis, we pooled results from 8 experiments each for INH, EMB, and 5-Cl-PZA treatments and untreated controls and calculated a Z-score for each identified protein between drug-treated and untreated cells.

Clustering of Proteins by Their Expression Profiles. Protein expression profiles were calculated from the relative abundance (f_i values) for proteins identified more than 20 times across the 60 shotgun proteomics experiments. Hierarchical clustering was performed on the mean-centered profiles using the program Cluster and displayed with the program Treeview.[35]

Functional Annotation of *M. smegmatis* Proteins. Functional annotation of the custom *M. smegmatis* predicted protein database was previously described.[16] Briefly, the proteins were assigned functional categories with the Clusters of Orthologous Groups (COG) database annotation[36] associated with their top BLAST hits with expectation value $< 1 \times 10^{-6}$ against a database of 89 fully sequenced genomes. *M. smegmatis* proteins were also assigned with *M. tuberculosis* orthologs' Gene Ontology (GO) functional annotation, where orthologs were identified as bidirectional best BLAST hits.

We calculated the enrichment of functional categories among proteins showing significantly differential expression in drug treatments. Under the hypergeometric distribution, the probability of a functional category being present only at levels expected by random chance was calculated as

$$F(k|n, M, N) = \sum_{i=k+1}^{\min(M,n)} P(i|n, M, N)$$

where

$$P(k, |n, M, N) = \frac{\binom{M}{k}\binom{N-M}{n-k}}{\binom{N}{n}}$$

and N is the total population size, M is the number of proteins in the functional category j, n is the number of identified proteins showing significant differential expression in that drug treatment, and k is the overlap between M and n. COG functional categories with $P_{integrated} < (1/18)$ were selected as significant, as there are 18 COG categories in *M. smegmatis*.

With the use of a two-tailed binomial distribution, we identified GO functional categories showing significant enrichment among proteins differentially expressed in drug treatments as

$$F(k|n, p) = \sum_{i=k+1}^{n} \binom{n}{I} p^i (1-p)^{n-i}$$

where n represents the total number of the identified proteins, k is the number of identified proteins with the functional category j, and p is the fraction of proteins in the functional category j for the whole genome. The enrichment of a functional category was calculated as $f = k/(N \cdot p)$, where N represents the total number of the identified proteins, k is the number of identified proteins with the functional category j, and p is the fraction of proteins in the functional category j for the whole genome. GO functional categories with $F < (1/350)$ were selected as significant, as there are 350 GO categories. For rare GO functional categories with $p < 0.05$, we calculated the significance based on Poisson statistics as

$$F(k|n, p) = e^{-p \cdot n}\left(\sum_{i=0}^{k} \frac{(p \cdot n)^k}{i!}\right)$$

where n, k, and p are defined as above. Again, GO functional categories with $F < (1/350)$ were selected as significant.

Results and Discussion

The Growth of *M. smegmatis* Cells Is Inhibited by Anti-TB Drugs. To investigate drug-induced metabolic changes, *M. smegmatis* protein expression was examined throughout a time course after adding the anti-TB drugs. The *M. smegmatis* mc^2155 cells were grown at 37 °C to early log phase, anti-TB drugs were added, and cells were grown with agitation at 37 °C. At initial time points, cells grew normally; with increasing time, cell growth slowed. In the presence of 4 μg/mL INH, the growth of *M. smegmatis* was reduced, and at 8 μg/mL, INH almost fully inhibited growth after 18 h. In EMB treatment, cell growth was decreased at an EMB concentration of 1 μg/mL and markedly reduced in 4 μg/mL EMB. 5-Cl-PZA slowed cell growth at a concentration of 25 μg/mL, although still did not fully inhibit cell growth with 50 μg/mL, consistent with previous observations.[8] Cells were harvested from each of these drug treatments and their proteomes analyzed by shotgun proteomics.

Proteins Identified in LC/LC/MS/MS Experiments. Approximately 1.6 million MS/MS peptide fragmentation spectra were collected and analyzed over the course of 33 LC/LC/MS/MS experiments, characterizing the proteins expressed in 33 samples drawn from time courses of *M. smegmatis* growing in three different drug (INH, EMB, 5-Cl-PZA) treatments. By integrating these data with 850 000 MS/MS spectra from 27 untreated control experiments,[16] we identified a total of 2550 *M. smegmatis* proteins. Proteins were identified using ProteinProphet[31] at an estimated false-positive identification rate of approximately 5%. These identified proteins represent ~40% of the ~6500 genes expected in the *M. smegmatis* genome (personal communication, David Graham), whose final sequence and annotation is currently underway at the J. Craig Venter Institute.

The Global Protein Expression Response of *M. smegmatis* to Anti-TB Drugs. It has been observed that the number of MS/MS spectra associated with each identified protein in shotgun proteomics experiments correlates well with protein concentrations.[37–39] In the 'spectral counting' approach, we consider the count of all MS/MS spectra from all peptides attributable to a given protein divided by the count of all interpreted MS/MS spectra for all proteins in the experiment. The resulting frequencies of MS/MS spectra have been shown to provide good estimates of relative protein abundance.[40,41] We estimated the relative protein abundance for each protein in drug-treated *M. smegmatis* cells using this approach (Supplementary Table 1 in Supporting Information). Protein expression profiles derived from the fraction of identified MS/MS spectra per protein reveal general trends of protein expression across the treatments (Figure 2). Proteins involved in drug target pathways generally cluster together in this analysis. INH's target 3-oxoacyl-acyl carrier protein synthase 2 (KasB) is in the same operon as 3-oxoacyl-acyl carrier protein synthase 1 (KasA), meromycolate extension acyl carrier protein (AcpM), malonyl CoA-acyl carrier protein transacylase (FabD), and acetyl/propionyl-CoA carboxylase (AccD6) (Figure 3C). We observed that proteins encoded by genes in this operon, which are involved in the FAS-II fatty acid synthesis pathway, are coordinately up-regulated when cells are treated with INH. Fatty acid synthetase (Fas), propionyl-CoA carboxylase (AccD5), and acetyl-/propionyl-CoA carboxylase (AccA3), proteins in the mycolic acid synthesis pathway, are also coexpressed in this cluster as might be expected from the general perturbation to mycolic acid synthesis. In EMB treatments, the inosine-5′-monophosphate dehydrogenases GuaB1, GuaB2, and GuaB3

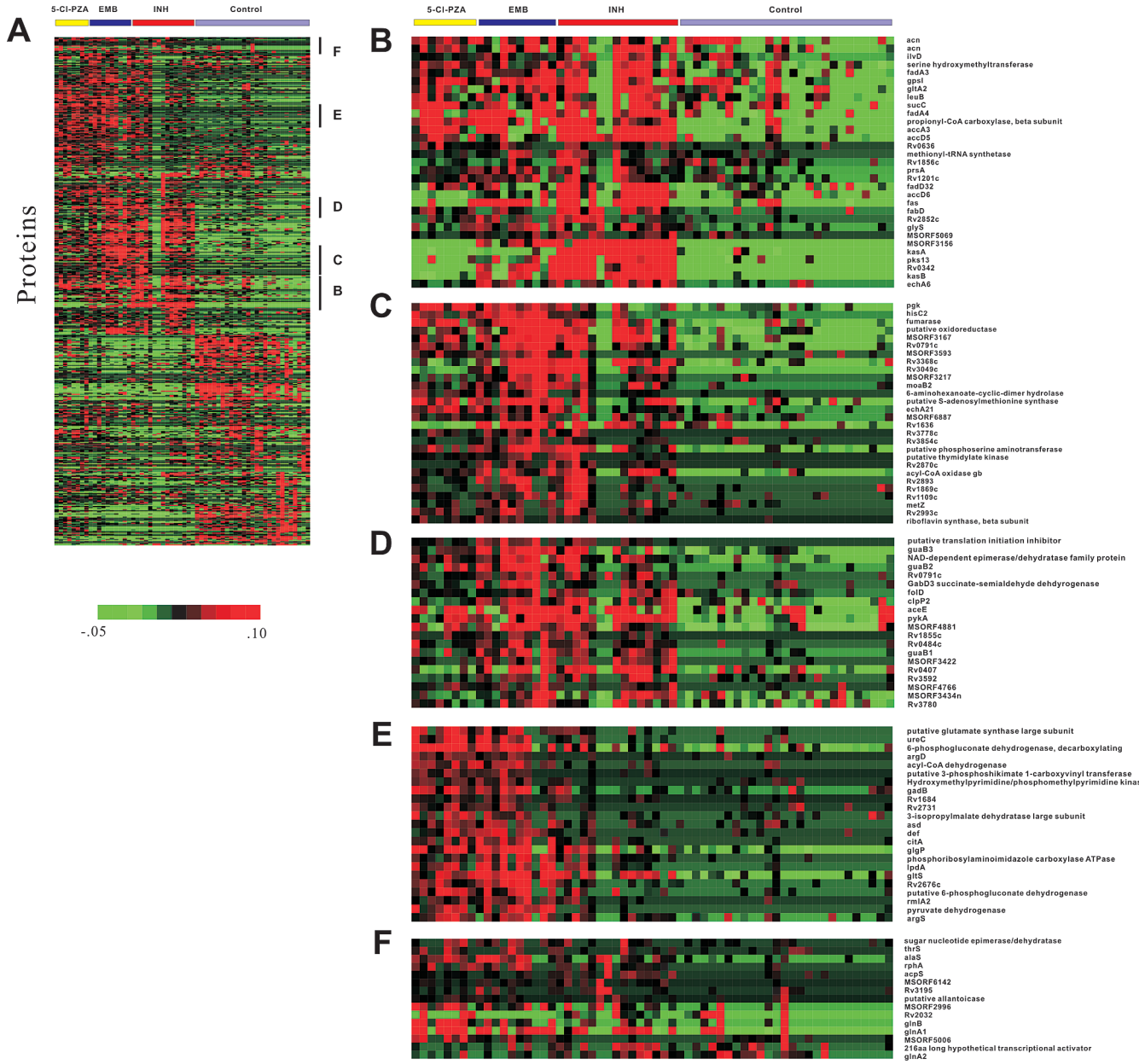

Figure 2. Hierarchical clustering of *M. smegmatis* proteins identified across 60 shotgun proteomics experiments. (A) Values in the matrix indicate the fractions of observed MS/MS spectra for 476 proteins (rows) identified more than 20 times across 60 shotgun experiments (columns). Black bars on the right indicate specific clusters expanded at right. (B−F) Among proteins with expression levels up-regulated in anti-TB drug treatments are those involved in the drug-target pathways.

are up-regulated. Glutamine synthetase GlnA and GlnB are up-regulated in 5-Cl-PZA treatment, which might be explained by 5-Cl-PZA-induced amide production activating the L-glutamine catabolism pathway.[42]

Operon-Encoded Proteins Change Expression Levels Coordinately. With these relative expression levels, we analyzed the expression of proteins encoded in the same operons. We see reasonably high coherence in the protein expression patterns of proteins in the same operon (Figure 3). For example, the expression levels of subunits of the F0F1-type ATP synthase (AtpF, AtpH, AtpA, AtpG, AtpD, and AtpC) are consistent across the three drug treatments and untreated controls (Figure 3A). Figure 3B shows that the proteins in the RpsJ and RpsS operons, components of the 11 gene S10 ribosomal protein operon, are strongly down-regulated in all three anti-TB drug treatments in a coordinate fashion. This result may indicate that these three drugs actively inhibit protein translation in cells or, more likely, may be a secondary effect of the cell growth inhibition. For the proteins in Figure 3, the average Pearson's correlation coefficient between adjacent proteins is 0.72, 0.96, 0.86, 0.99, and 0.74 for Figure 3, panels A−E; these correlations are significantly higher than random expectation based on non-adjacent genes ($p < 0.01$; Z-test).

We searched for operons that were up- or down-regulated in specific drug treatments. The proteins encoded by the KasB operon are strongly up-regulated in INH treatment (Figure 3C). KasB, the target of INH,[17] is in the same operon as KasA, AcpM, FabD, and AccD6, which are grouped into one coexpression cluster, except AcpM (Figure 2B). These proteins are known to be in the synthesis pathway for mycolic acid,[20] the main

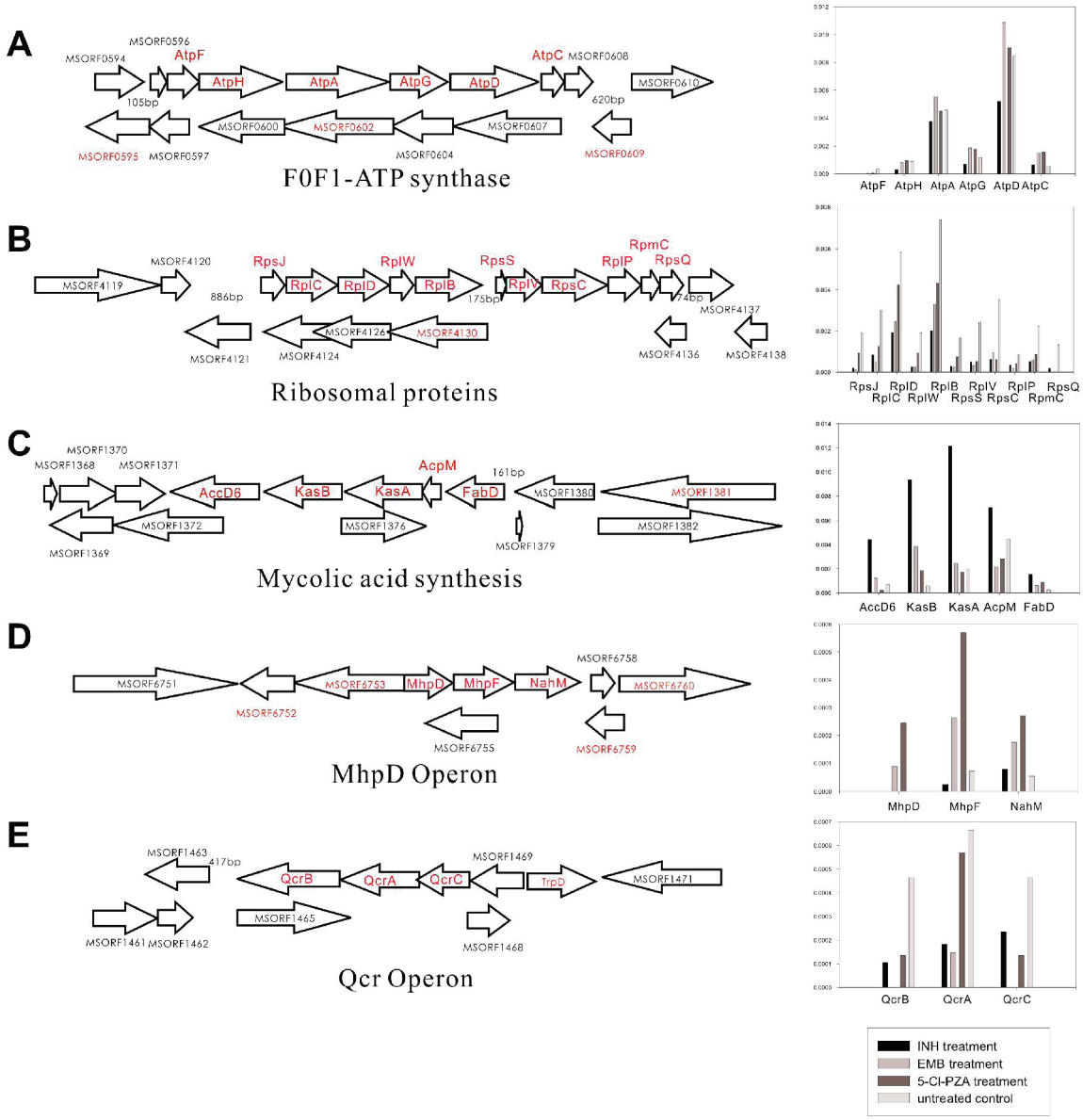

Figure 3. Levels of proteins encoded in the same operon change coordinately in drug treatments. Proteins labeled in red were identified in our experiments; proteins in bold red are in the same operon. Proteins in the ATPase operon (A) express consistently across all treatments; proteins in RpsJ, RpsS operons (B) are down-regulated in three drug treatments; the KasB operon (C), and the MhpD operon (D) are up-regulated in INH and 5-Cl-PZA treatments; proteins in the QcrABC operon (E) are down-regulated in EMB treatment. The *y*-axes in column charts (right) represent relative protein abundance, measured as the total number of observed MS/MS spectra associated with a given protein, expressed as a fraction of the total number of observed MS/MS spectra in the experiment.

component of the cell wall in mycobacteria, and have been previously observed to be significantly up-regulated in quantitative analysis of INH-induced proteomic changes measured by precursor intensity in LC/MS.[43] The INH-induced up-regulation of mycolic acid synthesis enzymes suggests the bacteria are up-regulating these enzymes to counteract the inhibitory effects of INH. Similarly, 2-keto-4-pentenoate hydratase (MhpD), acetyldehyde dehydrogenase (MhpF), and 4 hydroxy-2-oxovalerate aldolase (NahM) are up-regulated in 5-Cl-PZA treatment (Figure 3D). This operon is involved in catabolism of aromatic acids and amines;[44] the operon's specific induction in 5-Cl-PZA-treated cells may implicate this system or those functionally linked to it as 5-Cl-PZA targets. The ubiquinol-cytochrome C oxidoreductase QcrABC operon is down-regulated in EMB treatment (Figure 3E); this protein complex is an integral membrane enzyme that catalyzes electron transfer from a quinol to a c-type cytochrome.[45]

Protein Differential Expression in *M. smegmatis* in Anti-TB Drug Treatments. To characterize the specific response to each anti-TB drug, we measured differential expression of identified proteins by counting MS/MS spectra identified from each protein. The significance of differential expression was calculated as a *Z*-score from the difference in the number of identified MS/MS spectra for a given protein between two experiments.[33,34] The *Z*-scores of identified proteins across 32 experiments were calculated comparing drug-treated cells to the untreated controls (Supplementary Table 2 in Supporting Information), and proteins showing significant expression changes were chosen at the 99% confidence level ($|Z| \geq 2.58$). These differential protein profiles provide information on which

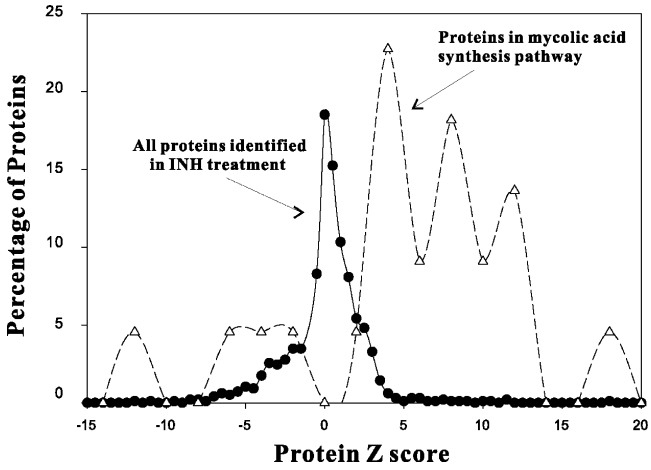

Figure 4. Proteins in the INH target pathway show differential expression during INH treatment and can be detected by their higher *Z*-scores, supporting the use of the *Z*-scores for the identification of candidate downstream targets in the 5-Cl-PZA and EMB experiments. Solid circles represent the distribution of *Z*-scores among all proteins identified after INH treatment; empty triangles represent *Z*-scores for proteins in the pathway of mycolic acid synthesis.

proteins are responsive in drug treatments and may belong to drug target pathways.

We evaluated this strategy by calculating differential protein expression for INH-treated cells, then testing how the known targets in the mycolate biosynthesis pathway behaved. Figure 4 shows that mycolic acid biosynthetic proteins are effectively identified by this strategy. While most cellular proteins are in the range of $|Z| < 2$, all of the 22 mycolic acid biosynthetic proteins show $|Z| > 2$, with the majority (18 proteins) up-regulated. In INH treatment, downstream targets of INH were effectively identified using *Z*-score. On the basis of this analysis, we might therefore expect that the proteins with high *Z*-score (or low *Z*-score) in EMB and 5-Cl-PZA experiments are also likely to be enriched in downstream targets of the drugs.

Using this strategy, we tested for proteins strongly up- or down-regulated in each drug treatment. Across 32 experiments, we identified 485 proteins differentially expressed with 99% confidence ($|Z| \geq 2.58$) from untreated controls. Each significantly differentially expressed protein was associated with a functional category, and the enrichment for particular functional categories was calculated. These enriched categories provide biological interpretation of the mass spectrometry-based measurement of differential expression. Functional enrichment for each drug treatment is shown in Figure 5. Translation, energy production, and protein export are down-regulated in all three drug treatments. These three drugs each inhibit cell growth (Figure 5B), apparent in the interruption of basic cellular processes. INH up-regulates lipid transport and metabolism 1.2-fold (Figure 5A), as expected for cells whose fatty acid synthesis (FASII) and mycolic acid synthesis are inhibited by INH. Lipid transport and metabolism is also up-regulated in EMB and 5-Cl-PZA treatments, in accordance with previous observations.[2,5,8] In addition, amino acid metabolism and transport is up-regulated in INH and 5-Cl-PZA treatments.

Figure 6 presents a visual summary of the drug-induced differential expression of 485 proteins against untreated controls as measured in the 32 experiments. For each protein, a point is plotted within the triangle at a position signifying the relative enrichment of the protein across three drug treatments. The relative peptide fractions in the three drug treatments were normalized to add up to 1 in order to indicate the relative expression, each fraction calculated as

$$f_{\mathrm{drug},i} = \frac{\mathrm{Fraction}_{\mathrm{drug},i}}{\sum_{\mathrm{all\_drugs},i} \mathrm{Fraction}_{j,i}}$$

where $\mathrm{Fraction}_{\mathrm{drug},i}$ represents the fraction of total interpreted MS/MS spectra that were derived from the protein *i* in total peptides observed in that drug's shotgun proteomics experiments. Proteins plotted in the middle of the triangle are equally abundant in all three drug treatments, indicating general responses of the cells to drug treatments and growth inhibition. Proteins sitting in one of the corners are highly induced in one drug treatment, and proteins that appear along one of the edges are induced in only two of the three drug treatments. For example, proteins involved in mycolate biosynthesis (labeled as red squares) sit in the INH corner. For discussion below, proteins of interest in EMB treatment are plotted as blue squares, in 5-Cl-PZA treatment as green squares.

1. The Effect of INH. Using Figure 6, we first summarize the proteins specifically induced in INH-treated cells. Proteins plotted in the INH-specific corner are involved in the biosynthesis of mycolic acid.[15,46] These proteins include the INH targets KasB and enoyl-acyl carrier protein reductase (InhA).[13] Alkylhydroperoxidase (AhpD, an element of the peroxiredoxin defense against oxidative stress), mycolic acid synthase (UmaA1), and acetyl-CoA acyltransferase (FadA2, involved in lipid degradation) are in the corner as up-regulated. In addition, proteins in FAS-II system, such as, KasA, AcpM, FabD, AccD6, polyketide synthase (Pks13), fatty-acid-CoA ligase (FadD32), and 3-oxoacyl-acyl carrier protein reductase (FabG4), are up-regulated, as expected in INH treatment.[46] The increased protein production presumably results in accumulated fatty acid pathway precursors. Fatty acid synthetase (Fas), which catalyzes the formation of long-chain fatty acids, is up-regulated. The isoniazid inducible protein (IniA),[47] essential for the activity of an efflux pump that confers drug tolerance to both INH and EMB, is also up-regulated. The INH up-regulation of the enzymes in the FASII system, seen in the proteomics data, suggests that the induction of these proteins is the consequence of a regulatory feedback mechanism in which the bacteria up-regulate mycolic acid synthesis enzymes to compensate for the inhibitory effects of INH.

Peroxidase/catalase (KatG), which activates INH, is strongly down-regulated. The end products of the mycolic acid pathway, the mycolyltransferases FbpA, B, and C, are down-regulated, which is consistent with previous observations.[20,48] This indicates that INH treatment progressively depletes mature mycolates.[20]

2. The Effect of EMB. Next, we summarize specific responses to EMB. EMB targets the mycobacterial cell wall, specifically the arabinosyl transferases EmbABC, which act to polymerize arabinose into the arabinan of arabinogalactan (AG) and lipoarabinomannan,[11] the major polysaccharides of the mycobacterial cell wall.[5–7] In our experiments, proteins involved in the FASII system are up-regulated in EMB treatments, such as KasB, Pks13, and Fas. In contrast, FbpA and FbpC are down-regulated, consistent with EMB indirectly inhibiting mycolic acid synthesis by limiting the availability of arabinan for attachment of the mycolic acids,[49] thereby triggering a cascade of changes in the lipid metabolism of mycobacteria.

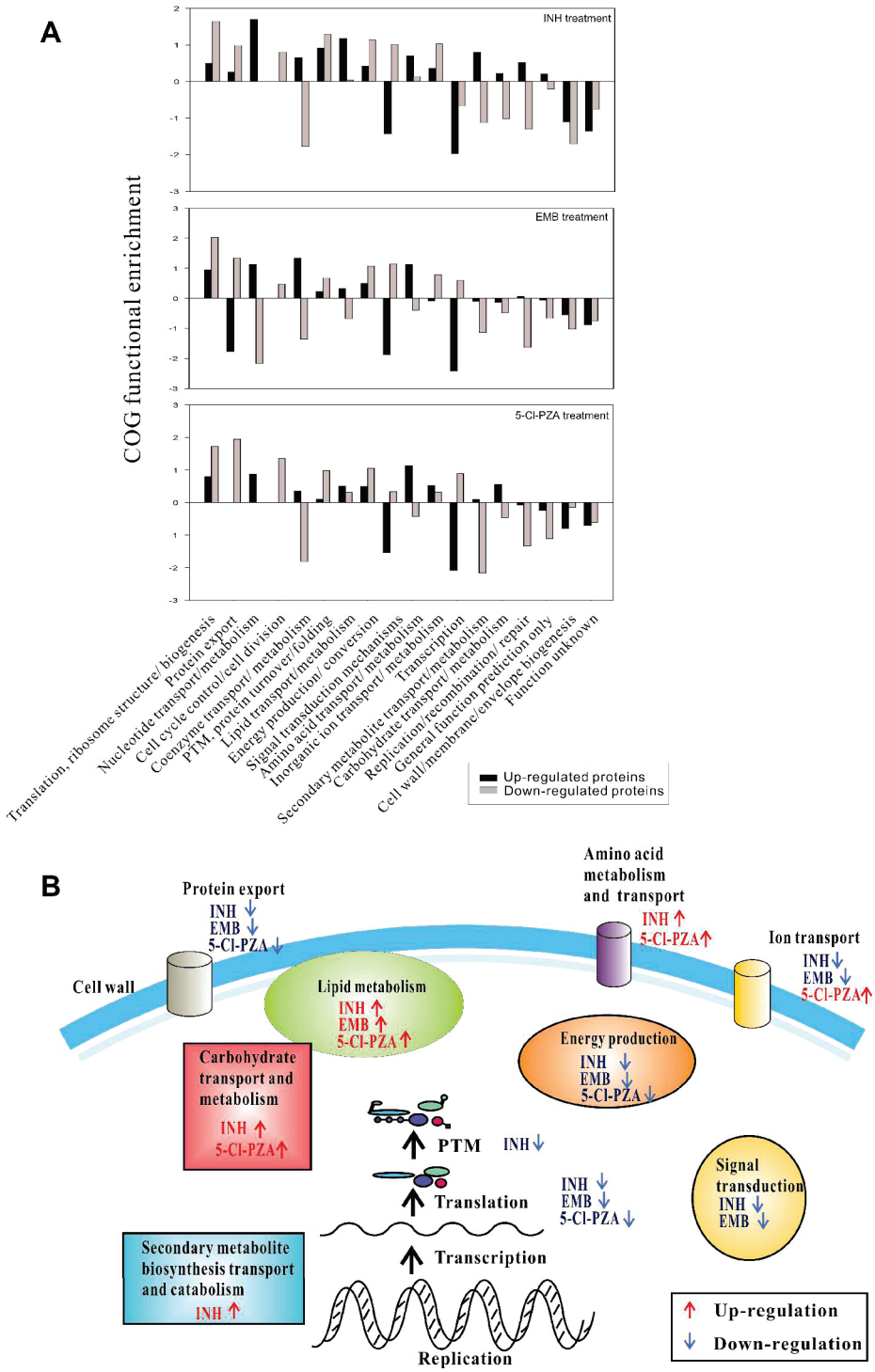

Figure 5. A pathway-level summary of protein expression level changes after drug treatments. A total of 485 proteins were selected as significantly differentially expressed with 99% confidence. (A) COG functions for the differentially expressed proteins in each drug treatment. Black bars represent up-regulated proteins ($Z \geq 2.58$) in the drug treatment; gray bars represent down-regulated proteins ($Z \leq -2.58$). For the proteins in each COG category, we plot the relative difference in expression level, calculated as $\log[(N_{up,COG_j}/N_{up})/(N_{COG_j}/N)]$, where N_{up,COG_j} and N_{up} represent the number of up-regulated proteins with COG_j function and the number of up-regulated proteins in each drug treatment, and N_{COG_j} and N are the number of observed proteins with COG_j function and the number of observed proteins for each drug treatment. PTM, post-translational modification. (B) The significant functional enrichments are illustrated, as calculated using the hypergeometric distribution. Red arrows represent proteins whose expression levels were up-regulated in a given drug treatment, blue arrows represent down-regulation.

In Figure 6, seven membrane proteins are specifically induced in EMB treatment, including penicillin-binding proteins (essential membrane bound cell wall synthesizing enzyme), aspartate racemase (cell wall biogenesis), transmembrane alanine and glycine rich protein (peptidoglycan biosynthesis), lipoprotein (LpqG), and the transmembrane cytochrome C oxidase CtaC (aerobic respiration). Maltooligosyltrehalose synthase (GlgY, involved in trehalose biosynthesis),

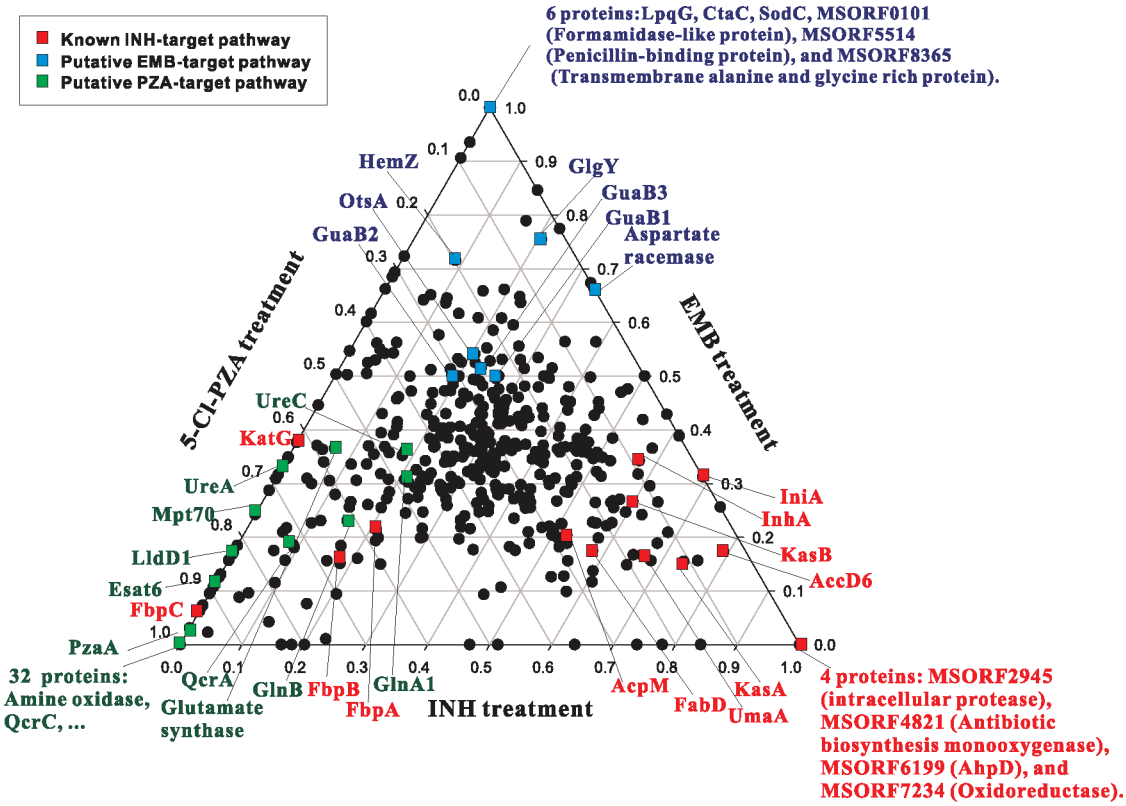

Figure 6. Drug treatment-specific protein expression changes, illustrated with a three-way comparison of relative protein abundance after INH, EMB, and 5-Cl-PZA treatments. Each dot represents the relative abundance of a protein in the three drug treatments, positioned so that proximity to a vertex is proportional to the level of enrichment in the respective sample. Colored squares are annotated proteins: red squares represent known proteins in INH pathway (mycolic acid synthesis pathway); blue squares represent proteins discussed in the results of the EMB experiments; green squares are proteins discussed in the results of the 5-Cl-PZA treatment.

enoyl-CoA hydratase (beta oxidation of fatty acids), and cystathionine/methionine gamma-synthase/lyase are also up-regulated specifically, as is ferrochelatase (HemZ), sharing an operon with two genes (MabA and InhA) involved in mycolic acid biosynthesis. Glutamyl-tRNA synthetase (GltS) and IMP dehydrogenase (GuaB1, Gua2, Gua3, involved in GMP biosynthesis) are up-regulated, presumably as glutamate and cAMP are necessary for galactose to be incorporated into the cell wall.[50] The induction of glutamate-1-semialdehyde 2,1-aminonutase (HemL) might be explained from the effect of EMB to increase glutamate efflux.[51] The remaining up-regulated EMB-specific proteins include zinc metalloprotease, monooxygenase (MSORF3583 and MSORF 2318), and oxidoreductase (LpdA and MSORF8662), as well as pyruvate carboxylase (Pca).

3. The Effect of PZA. Finally, we summarize the specific responses to 5-Cl-PZA. PZA is a prodrug, which has to be activated in *M. tuberculosis* cell by the pyrazinamidase/nicotinamidase (PncA), mutations in which confer resistance to PZA.[52] The active derivative of PZA is pyrazinoic acid, which is preferentially accumulated in acidic pH,[53] resulting in cell death. Relatively little is known about the targets of PZA, although PZA inhibits L-tryptophan catabolism[54] and increases catabolism of L-glutamine.[42] PZA blocks energy transport by disrupting membrane functions.[2,8] PZA has also been shown to inhibit fatty acid synthesis[9,55] and elevate the NAD^+ level in cells.[56]

Notable among proteins specifically up-regulated in 5-Cl-PZA treatment is PzaA, a homologue of PncA. As *M. smegmatis* apparently lacks the PncA gene, it seems likely from these data that PzaA is carrying out PncA's function in activating 5-Cl-PZA. Also up-regulated are glutamine synthetase GlnA1 (one of 4 copies of GlnA) and GlnB, which play a central role in nitrogen metabolism and the formation of a poly L-glutamate/glutamine cell wall structure,[57] as well as being responsible for NH_2^+ and energy status.[42] The subunits of urea amidohydrolase (UreA and UreC) are up-regulated; these widely conserved proteins serve to degrade amines[58] and may act here as a cellular defense against 5-Cl-PZA. In addition, MSORF2805 (Rv1626 ortholog, nitrogen regulation protein), cyanate lyase LlD1, formamidase, isocitrate dehydrogenase (Icd2), and MSORF1225 (Rv0462 ortholog, involved in energy production) are up-regulated, all of these proteins involved in nitrogen regulation and energy metabolism. Other up-regulated proteins include amine oxidase, amino acid transport system protein, aminotransferase, and oxidoreductase. We note also that the pH of the 5-Cl-PZA experiment is lower (5.6) than that of the control experiments (7), necessary for 5-Cl-PZA activation and to bring the 5-Cl-PZA MIC within an accessible range. Nonetheless, the proteins up-regulated in this treatment are not transcriptionally induced in *M. tuberculosis* grown under similar acidic conditions in the absence of the drug,[59] indicating that the protein expression changes we observe are drug-induced, not pH induced.

To further investigate 5-Cl-PZA effects, we plotted the expression changes of the significantly differentially expressed proteins ($|Z| \geq 2.58$) in the 5-Cl-PZA drug treatment as a function of their GO functional categories (Figure 7). We expect the most enriched categories might correspond to the pathways of 5-Cl-PZA drug targets. Among up-regulated proteins, carboxylic acid metabolism, organic acid metabolism, nitrogen

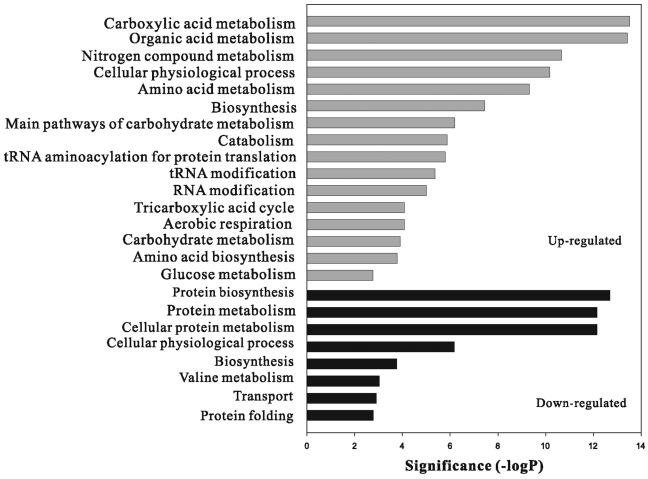

Figure 7. The significant GO functional categories of proteins identified as significantly differentially expressed ($|Z| \geq 2.58$) in 5-Cl-PZA treatments. The *x*-axis represents the logarithms of the hypergeometric-based probabilities for the significance of the GO category among differentially expressed proteins. Gray bars represent GO functional categories for the 89 significantly up-regulated proteins; black bars represent GO functional categories for the 71 significantly down-regulated proteins.

compound metabolism, and amino acid metabolism are significantly over-represented. In contrast, the GO pathways of protein biosynthesis and protein metabolism are significantly enriched among down-regulated proteins. It would appear from the proteomics data that PZA's primary specific effects are to perturb cellular nitrogen metabolism, carboxylic acid, and organic acid metabolism, with specific perturbations to glutamine metabolism and amine degradation.

Global Properties of the Observed Proteome. Finally, the shotgun proteomics data generated in these experiments also provide an efficient method for annotating the expressed proteome. In all, we provide experimental support for 2550 proteins (Supplementary Figure 1 in Supporting Information). Their COG categories (Supplementary Figure 1A in Supporting Information) indicate significant enrichment for proteins of energy production (6.5%), amino acid transport and metabolism (6%), and lipid transport and metabolism (4.8%). However, the largest fraction is uncharacterized proteins (44%). There is a clear enrichment over random expectation (Supplementary Table 4 in Supporting Information) in proteins of protein biosynthesis, amino acid biosynthesis and metabolism, nucleotide biosynthesis and metabolism, and carbohydrate metabolism. Low-abundance proteins such as those of DNA recombination and RNA transcription are under-represented in the shotgun proteomics data. Additional proteomics evidence for these proteins might be generated by targeting transcription regulation or lower abundance proteins. Similarly, in this study, we focused on intracellular protein expression changes in response to drug treatment. However, we note that secreted proteins are often important in pathogenesis and virulence, and that a targeted analysis of secreted proteins would be a good complement to this work.

For each protein identified, we calculated the number of identified MS/MS spectra and examined the distribution of these values across the set of 2550 proteins (Supplementary Figure 2 in Supporting Information). While the majority of proteins were observed a small number of times, an appreciable fraction of the proteins (35%) had 10 or more repeat observations of associated MS/MS spectra, with the highest sampling observed for the protein Tuf, whose MS/MS spectra we observed a remarkable 5603 times; other highly sampled proteins include GroEL2, Fas, AccA3, glycerol kinase 2, and GlnA1. While in this paper we have considered relative protein expression changes, spectral counting can also be applied to measure absolute protein abundances (e.g., refs 33, 34, and 37–39). These data therefore also indicate that, in principle, protein expression levels spanning up to roughly 3–4 orders of magnitude can be measured by this approach.

Conclusions

To explore alterations in *M. smegmatis* protein profiles, we have, by using LC/LC/MS/MS, generated signature profiles of *M. smegmatis* in response to treatments with INH, EMB, and 5-Cl-PZA. The protein profiles of *M. smegmatis* during exposure to drugs are direct consequences of these drugs and provide us valuable information on the drugs' modes of action. We observed that these three drugs selectively induce changes in the expression of enzymes in the affected pathways, especially before a more generalized stress response ensues.

With the use of mass spectrometry, we observed many drug-specific protein expression changes. In INH treatment, proteins involved in mycolic acid synthesis pathway are differentially regulated; most are up-regulated, although several proteins are down-regulated, such as the mycolyltransferases FbpA, FbpB, and FbpC. Induced proteins could be predicted to either compensate for inhibition of the target pathway or respond to the toxic effect of the drug, and we expect that the protein profiles can serve as a fingerprint of a given drug's mode of action. In this case, we reason that the bacteria are up-regulating mycolate synthesis enzymes to counterbalance the inhibition effects of INH. It remains to be seen whether the pathways identified in 5-Cl-PZA treatment represent up-regulated targets or other cellular responses to the toxicity. However, they provide a starting point for furthering our understanding of the drug's mechanism of action and, therefore, to the development of more effective drugs against tuberculosis.

Acknowledgment. The authors acknowledge funding from the Welch Foundation (F-1515), Packard Foundation, NSF, and NIH. We thank John Prince for valuable discussion and Dr. Jeffery Cox from the University of California at San Francisco for the kind gift of 5-chloropyrazinamide. We thank the J. Craig Venter Institute (JCVI) for access to the preliminary *M. smegmatis* genome sequence data, obtained from the JCVI web site at http://www.jcvi.org and used by permission here. Sequencing of *M. smegmatis* was accomplished with support from the National Institute of Allergy and Infections Diseases (NIAID).

Supporting Information Available: Supplementary Table 1 lists the 2550 *M. smegmatis* proteins observed by LC/LC/MS/MS, their BLAST and COG annotation, and relative abundance. Supplementary Table 2 lists the 485 significantly differentially expressed *M. smegmatis* proteins, their BLAST and COG annotation, and *Z*-scores. Supplementary Table 3 provides the list of specific *M. smegmatis* peptides identified by LC/LC/MS/MS. Supplementary Table 4 reports functional biases among the 2550 proteins. Supplementary Figures 1 and 2 report trends among the functions and mass spectrometry sampling of the 2550 proteins. This material is available free of charge via the Internet at http://pubs.acs.org.

References

(1) Corbett, E. L.; Watt, C. J.; Walker, N.; Maher, D.; Williams, B. G.; Raviglione, M. C.; Dye, C. The growing burden of tuberculosis: global trends and interactions with the HIV epidemic. *Arch. Intern. Med.* **2003**, *163* (9), 1009–1021.

(2) Zhang, Y. The magic bullets and tuberculosis drug targets. *Annu. Rev. Pharmacol. Toxicol.* **2005**, *45*, 529–564.

(3) Mdluli, K.; Slayden, R. A.; Zhu, Y.; Ramaswamy, S.; Pan, X.; Mead, D.; Crane, D. D.; Musser, J. M.; Barry, C. E., III. Inhibition of a Mycobacterium tuberculosis beta-ketoacyl ACP synthase by isoniazid. *Science* **1998**, *280* (5369), 1607–1610.

(4) Takayama, K.; Wang, C.; Besra, G. S. Pathway to synthesis and processing of mycolic acids in Mycobacterium tuberculosis. *Clin. Microbiol. Rev.* **2005**, *18* (1), 81–101.

(5) Takayama, K.; Kilburn, J. O. Inhibition of synthesis of arabinogalactan by ethambutol in Mycobacterium smegmatis. *Antimicrob. Agents Chemother.* **1989**, *33* (9), 1493–9149.

(6) Deng, L.; Mikusova, K.; Robuck, K. G.; Scherman, M.; Brennan, P. J.; McNeil, M. R. Recognition of multiple effects of ethambutol on metabolism of mycobacterial cell envelope. *Antimicrob. Agents Chemother.* **1995**, *39* (3), 694–701.

(7) Mikusova, K.; Slayden, R. A.; Besra, G. S.; Brennan, P. J. Biogenesis of the mycobacterial cell wall and the site of action of ethambutol. *Antimicrob. Agents Chemother.* **1995**, *39* (11), 2484–2489.

(8) Zhang, Y.; Mitchison, D. The curious characteristics of pyrazinamide: a review. *Int. J. Tuberc. Lung Dis.* **2003**, *7* (1), 6–21.

(9) Zimhony, O.; Cox, J. S.; Welch, J. T.; Vilcheze, C.; Jacobs, W. R., Jr. Pyrazinamide inhibits the eukaryotic-like fatty acid synthetase I (FASI) of Mycobacterium tuberculosis. *Nat. Med.* **2000**, *6* (9), 1043–1047.

(10) Washburn, M. P.; Yates, J. R., III. Analysis of the microbial proteome. *Curr. Opin. Microbiol.* **2000**, *3* (3), 292–297.

(11) Jungblut, P. R.; Schaible, U. E.; Mollenkopf, H. J.; Zimny-Arndt, U.; Raupach, B.; Mattow, J.; Halada, P.; Lamer, S.; Hagens, K.; Kaufmann, S. H. Comparative proteome analysis of Mycobacterium tuberculosis and Mycobacterium bovis BCG strains: towards functional genomics of microbial pathogens. *Mol. Microbiol.* **1999**, *33* (6), 1103–1117.

(12) Schmidt, F.; Donahoe, S.; Hagens, K.; Mattow, J.; Schaible, U. E.; Kaufmann, S. H.; Aebersold, R.; Jungblut, P. R. Complementary analysis of the Mycobacterium tuberculosis proteome by two-dimensional electrophoresis and isotope-coded affinity tag technology. *Mol. Cell. Proteomics* **2004**, *3* (1), 24–42.

(13) Sinha, S.; Kosalai, K.; Arora, S.; Namane, A.; Sharma, P.; Gaikwad, A. N.; Brodin, P.; Cole, S. T. Immunogenic membrane-associated proteins of Mycobacterium tuberculosis revealed by proteomics. *Microbiology* **2005**, *151* (Pt 7), 2411–2419.

(14) Washburn, M. P.; Wolters, D.; Yates, J. R., III. Large-scale analysis of the yeast proteome by multidimensional protein identification technology. *Nat. Biotechnol.* **2001**, *19* (3), 242–247.

(15) Mawuenyega, K. G.; Forst, C. V.; Dobos, K. M.; Belisle, J. T.; Chen, J.; Bradbury, E. M.; Bradbury, A. R.; Chen, X. Mycobacterium tuberculosis functional network analysis by global subcellular protein profiling. *Mol. Biol. Cell* **2005**, *16* (1), 396–404.

(16) Wang, R.; Prince, J. T.; Marcotte, E. M. Mass spectrometry of the M. smegmatis proteome: protein expression levels correlate with function, operons, and codon bias. *Genome Res.* **2005**, *15* (8), 1118–1126.

(17) Banerjee, A.; Dubnau, E.; Quemard, A.; Balasubramanian, V.; Um, K. S.; Wilson, T.; Collins, D.; de Lisle, G.; Jacobs, W. R., Jr. inhA a gene encoding a target for isoniazid and ethionamide in Mycobacterium tuberculosis. *Science* **1994**, *263* (5144), 227–230.

(18) Telenti, A.; Philipp, W. J.; Sreevatsan, S.; Bernasconi, C.; Stockbauer, K. E.; Wieles, B.; Musser, J. M.; Jacobs, W. R., Jr. The emb operon, a gene cluster of Mycobacterium tuberculosis involved in resistance to ethambutol. *Nat. Med.* **1997**, *3* (5), 567–570.

(19) Jacobs, W. R., Jr.; Kalpana, G. V.; Cirillo, J. D.; Pascopella, L.; Snapper, S. B.; Udani, R. A.; Jones, W.; Barletta, R. G.; Bloom, B. R. Genetic systems for mycobacteria. *Methods Enzymol.* **1991**, *204*, 537–555.

(20) Wilson, M.; DeRisi, J.; Kristensen, H. H.; Imboden, P.; Rane, S.; Brown, P. O.; Schoolnik, G. K. Exploring drug-induced alterations in gene expression in Mycobacterium tuberculosis by microarray hybridization. *Proc. Natl. Acad. Sci. U.S.A.* **1999**, *96* (22), 12833–12838.

(21) Takiff, H. E.; Cimino, M.; Musso, M. C.; Weisbrod, T.; Martinez, R.; Delgado, M. B.; Salazar, L.; Bloom, B. R.; Jacobs, W. R., Jr. Efflux pump of the proton antiporter family confers low-level fluoroquinolone resistance in Mycobacterium smegmatis. *Proc. Natl. Acad. Sci. U.S.A.* **1996**, *93* (1), 362–366.

(22) Phetsuksiri, B. B. A.; Cooper, A. M.; Minnikin, D. E.; Douglas, J. D.; Besra, G. S.; Brennan, P. J. Antimycobacterial activities of isoxyl and new derivatives through the inhibition of mycolic acid synthesis. *Antimicrob. Agents Chemother.* **1999**, *43* (5), 1042–1051.

(23) Wade, M. M.; Zhang, Y. Anaerobic incubation conditions enhance pyrazinamide activity against Mycobacterium tuberculosis. *J. Med. Microbiol.* **2004**, *53* (Pt 8), 769–773.

(24) Miesel, L.; Weisbrod, T. R.; Marcinkeviciene, J. A.; Bittman, R.; Jacobs, W. R., Jr. NADH dehydrogenase defects confer isoniazid resistance and conditional lethality in Mycobacterium smegmatis. *J. Bacteriol.* **1998**, *180* (9), 2459–2467.

(25) Chen, P.; Bishai, W. R. Novel selection for isoniazid (INH) resistance genes supports a role for NAD+-binding proteins in mycobacterial INH resistance. *Infect. Immun.* **1998**, *66* (11), 5099–5106.

(26) DeBarber, A. E.; Mdluli, K.; Bosman, M.; Bekker, L. G.; Barry, C. E. 3rd, Ethionamide activation and sensitivity in multidrug-resistant Mycobacterium tuberculosis. *Proc. Natl. Acad. Sci. U.S.A.* **2000**, *97* (17), 9677–9682.

(27) Primm, T. P.; Andersen, S. J.; Mizrahi, V.; Avarbock, D.; Rubin, H.; Barry, C. E. 3rd. The stringent response of Mycobacterium tuberculosis is required for long-term survival. *J. Bacteriol.* **2000**, *182* (17), 4889–4898.

(28) Link, A. J.; Eng, J.; Schieltz, D. M.; Carmack, E.; Mize, G. J.; Morris, D. R.; Garvik, B. M.; Yates, J. R., III. Direct analysis of protein complexes using mass spectrometry. *Nat. Biotechnol.* **1999**, *17* (7), 676–682.

(29) Yi, E. C.; Marelli, M.; Lee, H.; Purvine, S. O.; Aebersold, R.; Aitchison, J. D.; Goodlett, D. R. Approaching complete peroxisome characterization by gas-phase fractionation. *Electrophoresis* **2002**, *23* (18), 3205–3216.

(30) Keller, A.; Nesvizhskii, A. I.; Kolker, E.; Aebersold, R. Empirical statistical model to estimate the accuracy of peptide identifications made by MS/MS and database search. *Anal. Chem.* **2002**, *74* (20), 5383–5392.

(31) Nesvizhskii, A. I.; Keller, A.; Kolker, E.; Aebersold, R. A statistical model for identifying proteins by tandem mass spectrometry. *Anal. Chem.* **2003**, *75* (17), 4646–4658.

(32) Prince, J. T.; Carlson, M. W.; Wang, R.; Lu, P.; Marcotte, E. M. The need for a public proteomics repository. *Nat. Biotechnol.* **2004**, *22* (4), 471–472.

(33) Lu, P.; Vogel, C.; Wang, R.; Yao, X.; Marcotte, E. M. Absolute protein expression profiling estimates the relative contributions of transcriptional and translational regulation. *Nat. Biotechnol.* **2007**, *25* (1), 117–124.

(34) Lu, P.; Rangan, A.; Chan, S. Y.; Appling, D. R.; Hoffman, D. W.; Marcotte, E. M. Global metabolic changes following loss of a feedback loop reveal dynamic steady states of the yeast metabolome. *Metab. Eng.* **2007**, *9* (1), 8–20.

(35) Eisen, M. B.; Spellman, P. T.; Brown, P. O.; Botstein, D. Cluster analysis and display of genome-wide expression patterns. *Proc. Natl. Acad. Sci. U.S.A.* **1998**, *95* (25), 14863–14868.

(36) Tatusov, R. L.; Natale, D. A.; Garkavtsev, I. V.; Tatusova, T. A.; Shankavaram, U. T.; Rao, B. S.; Kiryutin, B.; Galperin, M. Y.; Fedorova, N. D.; Koonin, E. V. The COG database: new developments in phylogenetic classification of proteins from complete genomes. *Nucleic Acids Res.* **2001**, *29* (1), 22–28.

(37) Ishihama, Y.; Oda, Y.; Tabata, T.; Sato, T.; Nagasu, T.; Rappsilber, J.; Mann, M. Exponentially modified protein abundance index (emPAI) for estimation of absolute protein amount in proteomics by the number of sequenced peptides per protein. *Mol. Cell. Proteomics* **2005**, *4* (9), 1265–1272.

(38) Liu, H.; Sadygov, R. G.; Yates, J. R., III. A model for random sampling and estimation of relative protein abundance in shotgun proteomics. *Anal. Chem.* **2004**, *76* (14), 4193–4201.

(39) States, D. J.; Omenn, G. S.; Blackwell, T. W.; Fermin, D.; Eng, J.; Speicher, D. W.; Hanash, S. M. Challenges in deriving high-confidence protein identifications from data gathered by a HUPO plasma proteome collaborative study. *Nat. Biotechnol.* **2006**, *24* (3), 333–338.

(40) Dong, M. Q.; Venable, J. D.; Au, N.; Xu, T.; Park, S. K.; Cociorva, D.; Johnson, J. R.; Dillin, A.; Yates, J. R., III. Quantitative mass spectrometry identifies insulin signaling targets in C. elegans. *Science* **2007**, *317* (5838), 660–663.

(41) Schmidt, M. W.; Houseman, A.; Ivanov, A. R.; Wolf, D. A. Comparative proteomic and transcriptomic profiling of the fission yeast Schizosaccharomyces pombe. *Mol. Syst. Biol.* **2007**, *3*, 79.

(42) Bugrim, A.; Nikolskaya, T.; Nikolsky, Y. Early prediction of drug metabolism and toxicity: systems biology approach and modeling. *Drug Discovery Today* **2004**, *9* (3), 127–135.

(43) Hughes, M. A.; Silva, J. C.; Geromanos, S. J.; Townsend, C. A. Quantitative proteomic analysis of drug-induced changes in mycobacteria. *J. Proteome Res.* **2006**, *5* (1), 54–63.
(44) Arai, H.; Yamamoto, T.; Ohishi, T.; Shimizu, T.; Nakata, T.; Kudo, T. Genetic organization and characteristics of the 3-(3-hydroxyphenyl)propionic acid degradation pathway of Comamonas testosteroni TA441. *Microbiology* **1999**, *145* (Pt 10), 2813–2820.
(45) Yu, J.; Hederstedt, L.; Piggot, P. J. The cytochrome bc complex (menaquinone:cytochrome c reductase) in Bacillus subtilis has a nontraditional subunit organization. *J. Bacteriol.* **1995**, *177* (23), 6751–6760.
(46) Raman, K.; Rajagopalan, P.; Chandra, N. Flux balance analysis of mycolic Acid pathway: targets for anti-tubercular drugs. *PLoS Comput. Biol.* **2005**, *1* (5), e46.
(47) Colangeli, R.; Helb, D.; Sridharan, S.; Sun, J.; Varma-Basil, M.; Hazbon, M. H.; Harbacheuski, R.; Megjugorac, N. J.; Jacobs, W. R., Jr.; Holzenburg, A.; Sacchettini, J. C.; Alland, D. The Mycobacterium tuberculosis iniA gene is essential for activity of an efflux pump that confers drug tolerance to both isoniazid and ethambutol. *Mol. Microbiol.* **2005**, *55* (6), 1829–1840.
(48) Cabusora, L.; Sutton, E.; Fulmer, A.; Forst, C. V. Differential network expression during drug and stress response. *Bioinformatics* **2005**, *21* (12), 2898–2905.
(49) H, L.; Laszlo, A.; Rastogi, N. Mode of action of antimycobacterial drugs. *Acta Leprol.* **1989**, *7* (Suppl. 1), 189–194.
(50) Raychaudhuri, S.; Basu, M.; Mandal, N. C. Glutamate and cyclic AMP regulate the expression of galactokinase in Mycobacterium smegmatis. *Microbiology* **1998**, *144* (Pt 8), 2131–2140.
(51) Radmacher, E.; Stansen, K. C.; Besra, G. S.; Alderwick, L. J.; Maughan, W. N.; Hollweg, G.; Sahm, H.; Wendisch, V. F.; Eggeling, L. Ethambutol, a cell wall inhibitor of Mycobacterium tuberculosis, elicits L-glutamate efflux of Corynebacterium glutamicum. *Microbiology* **2005**, *151* (Pt 5), 1359–1368.
(52) Scorpio, A.; Zhang, Y. Mutations in pncA, a gene encoding pyrazinamidase/nicotinamidase, cause resistance to the antituberculous drug pyrazinamide in tubercle bacillus. *Nat. Med.* **1996**, *2* (6), 662–667.
(53) Zhang, Y.; Scorpio, A.; Nikaido, H.; Sun, Z. Role of acid pH and deficient efflux of pyrazinoic acid in unique susceptibility of Mycobacterium tuberculosis to pyrazinamide. *J. Bacteriol.* **1999**, *181* (7), 2044–2049.
(54) Saito, K.; Fujigaki, S.; Heyes, M. P.; Shibata, K.; Takemura, M.; Fujii, H.; Wada, H.; Noma, A.; Seishima, M. Mechanism of increases in L-kynurenine and quinolinic acid in renal insufficiency. *Am. J. Physiol.: Renal Physiol.* **2000**, *279* (3), F565–572.
(55) Boshoff, H. I.; Mizrahi, V.; Barry, C. E., III. Effects of pyrazinamide on fatty acid synthesis by whole mycobacterial cells and purified fatty acid synthase I. *J. Bacteriol.* **2002**, *184* (8), 2167–2172.
(56) Shibata, K.; Fukuwatari, T.; Sugimoto, E. Effects of dietary pyrazinamide, an antituberculosis agent, on the metabolism of tryptophan to niacin and of tryptophan to serotonin in rats. *Biosci. Biotechnol. Biochem.* **2001**, *65* (6), 1339–1346.
(57) Harth, G.; Zamecnik, P. C.; Tang, J. Y.; Tabatadze, D.; Horwitz, M. A. Treatment of Mycobacterium tuberculosis with antisense oligonucleotides to glutamine synthetase mRNA inhibits glutamine synthetase activity, formation of the poly-L-glutamate/glutamine cell wall structure, and bacterial replication. *Proc. Natl. Acad. Sci. U.S.A.* **2000**, *97* (1), 418–423.
(58) Carpene, C.; Bour, S.; Visentin, V.; Pellati, F.; Benvenuti, S.; Iglesias-Osma, M. C.; Garcia-Barrado, M. J.; Valet, P. Amine oxidase substrates for impaired glucose tolerance correction. *J. Physiol. Biochem.* **2005**, *61* (2), 405–419.
(59) Fisher, M. A.; Plikaytis, B. B.; Shinnick, T. M. Microarray analysis of the Mycobacterium tuberculosis transcriptional response to the acidic conditions found in phagosomes. *J. Bacteriol.* **2002**, *184* (14), 4025–4032.

PR0703066